Hindawi
Journal of Nanomaterials
Volume 2022, Article ID 9861440, 15 pages
https://doi.org/10.1155/2022/9861440

Research Article

Reduced Graphene Oxide-Tailored $CuFe_2O_4$ Nanoparticles as an Electrode Material for High-Performance Supercapacitors

B. Carmel Jeeva Mary,[1] J. Judith Vijaya,[1] Radhika R. Nair,[1] A. Mustafa,[2] P. Stephen Selvamani,[1] B. Saravanakumar,[3] M. Bououdina,[4] and L. John Kennedy[5]

[1]*Catalysis and Nanomaterials Research Laboratory, Department of Chemistry, Loyola College, Chennai 600 034, India*
[2]*Department of Physics, College of Science, University of Bahrain, PO Box 32038, Manama, Bahrain*
[3]*Department of Physics, Dr. Mahalingam College of Engineering and Technology, Pollachi, Tamil Nadu 642 003, India*
[4]*Department of Mathematics and Science, Faculty of Humanities and Sciences, Prince Sultan University, Riyadh, Saudi Arabia*
[5]*Materials Division, School of Advanced Sciences, Vellore Institute of Technology (VIT), Chennai Campus, Chennai 600 127, India*

Correspondence should be addressed to J. Judith Vijaya; jjvijaya78@gmail.com

Received 21 December 2021; Revised 25 March 2022; Accepted 29 March 2022; Published 11 April 2022

Academic Editor: Valeri P. Tolstoy

Transition metal oxide-based magnetic nanocomposites attract great attention due to their unique properties and applications in the field of energy storage. Herein, we present a facile microwave procedure for the synthesis of $CuFe_2O_4$ (CF) and $CuFe_2O_4$ incorporated with reduced graphene oxide $CuFe_2O_4$/rGO (CG) as potential electrode materials for hybrid supercapacitor. The structure and morphology of CF and CG nanoparticles are examined. The electrochemical performance is studied in 6 M aqueous KOH electrolyte using cyclic voltammetry (CV), galvanostatic charge-discharge (GCD), and electrochemical impedance spectroscopy (EIS) techniques. The attractive CG nanocomposite exhibits high specific capacity of 800 C/g at a current density of 2 A/g and better cycling stability when compared to pure CF, due to the formation of nanostructure composed of ferrite nanoparticles homogeneously incorporated onto rGO sheets. Furthermore, the practicability of CG electrode is investigated by the fabrication of CG and activated carbon. The hybrid supercapacitor device shows excellent electrochemical performance with specific energy of 18.3 Wh/kg and a specific power of 455 W/kg. It is noteworthy that the cyclic stability is excellent with a capacity retention of ~98% after 3000 cycles manifesting the superiority of CG electrode. The proposed device demonstrates the potential to fabricate other metal oxides with activated carbon via a facile synthesis method for promoting application in energy storage materials and promoting new opportunities of binary nanocomposite.

1. Introduction

Nowadays, there is a high demand for discovering simple and novel approaches for generating efficient energy storage devices due to the fast development of advanced electronic gadgets [1]. As the worldwide population is completely dependent on electronic devices for the basic daily requirements, the need for energy storage systems is of utmost important that has led to extensive research endeavor for designing low-cost energy storage devices with excellent performances. Supercapacitors are a promising energy storage medium with exceptional properties, including very high power density, long cyclic stability, rapid charging-discharging, eco-friendly, and weightless material [2, 3]. In general, supercapacitors are classified into two types based on their charge storage mechanism. The electrochemical double-layer capacitor (EDLC) is composed of carbon materials where the charge is stored electrostatically, while in the pseudocapacitors, the charge is stored in faradic [4].

However, the search and development of an electrode material with desired properties remain a very challenging task for the manufacturing of high-performance supercapacitors. The transition metal oxides (TMOs) are the classic examples that have been utilized in the preparation of supercapacitor electrodes. In recent decades, RuO_2 has been used as the most assuring electrode material for supercapacitor

applications but its usage is confined due to its toxicity, high cost, and poor conductivity [5]. Furthermore, MnO_2 electrode suffers of poor oxidation state below 0 V and hence limited its usage. Currently, mixed transition metal oxides and hydroxides are considered as the primary source of high-performance pseudocapacitive electrode materials owing to the synergic effect caused by the presence of different chemical compounds. Wu et al. [6] designed cobalt-nickel hydroxides asymmetric high-performance flexible supercapacitors with a capacity of 929 C/g at a current density of 2 mA/cm. Tao et al. [7] prepared hierarchical structure of Co_3O_4 with a specific capacity of 226.1 C/g. Ma et al. synthesized high-performance nickel hydroxide nitrate with a capacitance of 563.9 C/g [8]. Zhu et al. [9] prepared aluminum-doped cobalt-nickel hydroxides which exhibit high specific capacity of 264 mAh/g.

Among the various TMOs, spinel ferrites (MFe_2O_4, where M = metal) have acquired enormous attention, thanks to their fascinating and tunable electrochemical, magnetic, electrical, optical, and resistive properties in the preparation of a pseudocapacitive electrode material. The combining effect of Fe and metal ions generates a rich redox reaction and consequently a higher specific capacity [10–12].

In recent years, several works have been reported on the use of copper ferrite, nickel ferrite, cobalt ferrite, zinc ferrite, and their graphene-based composites for supercapacitor applications [13]. Among the ferrites, copper ferrites are considered as one of the prominent transition metal oxides that can be employed for different applications owing to their low cost, high surface area, environment-friendly nature, energy storage, and catalytic reactions [14–17]. Aparna et al. performed a comparative study on the metal ferrites (MFe_2O_4, M = Fe, Ni, Co, Mn, Zn, and Cu) and reported higher specific capacitance of 250 F/g at a scan rate of 2 mV/s for Cu ferrite when compared with other metal ferrites [18].

Regardless of its distinguished properties and its favorable application in different fields, a limited number of articles are found in the literature. Till to date, copper ferrite has been effectively prepared by the solvothermal [19], coprecipitation [20], hydrothermal [21], and sol-gel combustion and microwave-assisted combustion method [22].

Jin et al. prepared $CuFe_2O_4$ coated with carbon-based nanoparticles by the hydrothermal method to improve the electrochemical performances on Li-ion battery [23]. Zhu et al. [14] also prepared $CuFe_2O_4$ by the hydrothermal method ($CuCl_2$ and $FeCl_3$ precursors, sodium acetate, and polyvinylpyrrolidone) with a specific capacitance (C) of 334 F/g at 0.6 A/g and with 85% capacitance retention at 1 A/g. Nonetheless, Khan et al. [24] found that $CuFe_2O_4$/Fe_2O_3 composite obtained by the coprecipitation method (copper nitrate, ferric nitrate, and polyethylene glycol) exhibited much higher capacitance of 638 F/g at 0.6 A/g with 66.4% capacitance retention at 1 A/g. Zhang et al. [25] used the solvothermal method to prepare $CuFe_2O_4$/rGO ($CuCl_2$, $FeCl_3$, NaAc, PVP, ethylene glycol, and GO) and reported a capacitance of 576.6 F/g at 1 A/g and 79.1% capacitance retention at 3 A/g. Similarly, Chandel et al. [26] prepared $CuFe_2O_4$/rGO by the coprecipitation method ($Cu(NO_3)_2$, $Fe(NO_3)$, 30 mL GO suspension in water, and 2 M NaOH) with the best performance so far; i.e., a capacitance of 797 F/g at 2 A/g and 92% capacitance retention at 6 A/g and a cyclic stability of 2000 cycles. Xing et al. prepared $CuFe_2O_4$ by a solid-state reaction and attained capacitance of 950 mAh/g at 100 mA/g and exhibit better cyclic performance after 60 cycles [27].

However, Elayappan et al. reported that the low sensitivity of spinel $CuFe_2O_4$ is improved by the a carbon-based material [28]. Also, the low electrochemical activity of $CuFe_2O_4$ is due to insufficient electron conductivity which can be modified by the addition of a conducting material [29]. The attractive properties of graphene such as high surface area, two-dimensional sp^2 carbon atoms, low density, and exceptional electrical conductivity have received enormous attention in diverse applications primarily when decorated with nanoparticles. Specifically, the high charge carriage mobility and specific surface area of graphene offer broad range of applications such as in catalysis, sensors, drug delivery, solar panels, DNA sequencing, electronics, and energy storage [30, 31]. It has been reported that the enhanced electrochemical activity of the graphene-based electrode is due to the presence of several functional groups at the edge planes in the graphene sheet [32].

Typically, graphite oxide (GO) can be readily reduced to reduced graphene oxide (rGO) by different reduction methods such as thermal, hydrazine-assisted Hummer's method, or photochemical reduction [33]. It is important to highlight that rGO possesses higher stability and conductivity in organic solvents and better electrochemical characteristics (supercapacitors) resulting in higher performance. In this context, this study primarily focuses on exploiting these interesting properties of graphene in the design of ferrite-graphene-based nanocomposite to achieve enhanced electrode' performance.

Lou et al. [34] and Chen et al. [35] prepared N, O, and cobalt-doped 2D carbon nanosheet for zinc ion hybrid supercapacitors using natural products by the combustion method, showing excellent electrochemical activity. Thatikayala and Min [36] successfully synthesized copper ferrite/rGO using the biocombustion method to improve the electrochemical properties. In the literature, the solution combustion synthesis is a commonly used technique which uses dissolved solutions of metal nitrates and fuels to undergo exothermic reaction. It is noteworthy that the synthesis of $CuFe_2O_4$ and $CuFe_2O_4$/rGO nanocomposite by the microwave-assisted combustion method could be achieved successfully in the preparation of both organic and inorganic materials [37–39]. This is mainly due to its advantages in obtaining pure nanosized particles in shorter reaction time with high chemical yield [40]. The generation of heat energy in microwave reactor occurs by internal heating where the microwave energy is converted into heat energy by strong intermolecular friction and helps to increase the temperature of the precursors [41]. As a result, the crystallite size, texture, morphology, surface area, and other physicochemical properties will be largely altered. Besides, the use of microwave energy as a heating source accelerates the chemical reaction and kinetics to improve the economic viability and reduces the energy loss [42].

Furthermore, fuel plays a major role in the combustion reaction, because during the exothermic reaction, oxidation of the fuel takes place liberating CO_2, H_2O, and N_2 gases. This leads to the breakdown of large particles to form combusted ash that contains many pores. The size and volume of the pores are predominantly controlled by the fuel and its composition [43].

This study is aimed at stabilizing the surface properties of $CuFe_2O_4$ and $CuFe_2O_4$/rGO nanocomposite by using lysine amino acids as fuel. Amino acids are biologically essential and nontoxic compounds having the potential to manipulate the surface morphology of nanoparticles [44]. It is interesting to mention here that the adsorption phenomenon takes place between the amino acids and iron oxide by the formation of chelate chemical bonds involving the carboxylate group and surface of Fe (III) [45]. Amino acids can act as a surfactant employed in mass preparation of nanoparticles and can change the surface features, because of the availability of wide range of functional groups. From the previous works, compounds like urea, aspartic acid, alanine, glycine, citric acid, L-alanine, and carbohydrazide have been used in a proper stoichiometric ratio and act as fuels to control the combustion process in accordance with the propellant chemistry principle [46]. L-lysine ($C_6H_{14}N_2O_2$) is one of the amino acids with a high reducing power of +34 when compared to other conventional amino acids like urea (+6) and glycine (+9) [47]. L-lysine is also found to promote the uniform mixing of cations in the reaction mixture and facilitates the combustion. To the best of knowledge of the authors, no previous studies have been conducted on the synthesis of copper ferrite and copper ferrite/rGO nanocomposite using L-lysine.

Herein, a novel facile microwave-assisted combustion method has been employed to synthesize copper ferrite and copper ferrite/rGO nanocomposite with L-lysine as a fuel. The as-prepared nanostructures were examined by means of XRD, FT-Raman, FT-IR, and SEM-EDX and HR-TEM and then tested as supercapacitor electrode materials.

2. Experimental Section

2.1. Preparation of $CuFe_2O_4$ Nanoparticles. The samples were prepared using AR-grade copper nitrate (99% purity), ferric nitrate (99% purity), and L-lysine (99% purity) purchased from Merck and used without further purification. Double distilled water (DDW) was used throughout the synthesis. In the present work, $CuFe_2O_4$ sample was synthesized via the microwave-assisted combustion method. 1 M Cu $(NO_3)_2.3H_2O$ and 2 M $Fe(NO_3)_3.9H_2O$ were used as cation precursors, and L-lysine amino acid was used as a fuel. The prepared molar ratio of nitrates is 1 : 2 and nitrates to amino acid is 1 : 1. The as-obtained solutions were mixed and magnetically stirred for about 24 h at room temperature. Finally, the homogenous solution was subjected to microwave irradiation for about 12 min at 800 W, and the obtained black powder was labeled as CF.

2.2. Preparation of $CuFe_2O_4$/rGO Nanocomposite. Reduced graphene oxide (rGO) was prepared by the modified Hummer method [48]. $CuFe_2O_4$/rGO composites were prepared as follows: 10 mg GO was dispersed in H_2O and stirred continuously to form vigorous homogenous solution. To this solution, 1 M $Cu(NO_3)_2$, 2 M $Fe(NO_3)_3$, and lysine fuel were added and kept under magnetic stirring for 24 h. The obtained solution was transferred to 150 mL crucible and kept in a domestic microwave oven (2.45 GHz, 800 W) for 15 min. The obtained black precipitate $CuFe_2O_4$/rGO was washed with distilled water and ethanol and then labeled as CG. A schematic representation which is involved in the formation of $CuFe_2O_4$/rGO nanocomposite is given in Figure 1.

2.3. Structural and Morphological Characterization. X-ray diffraction patterns were recorded using a Bruker D8 diffractometer equipped with CuKα radiation source ($\lambda = 1.5418$ Å). The morphology of the sample was checked by scanning electron microscopy (FESEM) using Zeiss Ultra 55 equipped with Oxford EDS for elemental chemical composition and by transmission electron microscopy (TEM) using JEM 1400 Plus JOEL. FT-Raman analysis was carried out using a Bruker RFS 27: stand-alone FT-Raman spectrometer. FTIR measurements were conducted using a PerkinElmer infrared spectrophotometer (Waltham, MA, USA) in the range 4000–400 cm^{-1}.

2.4. Electrochemical Measurement. In the current study, the electrochemical measurements were conducted using a CHI660C electrochemical analyzer. A three-electrode cell of platinum wire as counter electrode, Ag/AgCl as reference electrode, and nickel foam coated with the active material working electrode was formulated. Herein, the active materials are $CuFe_2O_4$ and $CuFe_2O_4$/rGO. A semifluid blend was prepared by mixing the active material, carbon black, and polyvinylidene difluoride in the ratio of 8 : 1 : 1. About 2 mg of the blend was uniformly coated on the designed nickel foam (1 cm × 1 cm × 0.2 mm) which was air dried using a hot air oven at 80°C for 12 h.

The electrochemical tests were performed with the electrolyte solution of 6 M KOH. Cyclic voltammetry (CV) measurements were examined with the working potential window between 0 and 0.5 V and a scan rate in the range 10-100 mV/s. Galvanostatic charge-discharge (GCD) measurements were carried out at different current densities varying from 2 to 10 A/g to study the specific capacity (C) of the as-prepared sample. The specific capacity was calculated using the following equation:

$$C_g = \frac{I \times \Delta t}{m \times 3.6} \left(\frac{C}{g}\right), \quad (1)$$

where I (A) is the charge-discharge current (mA), Δt is the discharge time (s), and m is the mass of the active material (mg).

Electrochemical impedance spectroscopy (EIS) was examined to analyze the resistive and capacitive measurements of the electrodes in the frequency ranging from 0.01 Hz to 100 kHz. The specific energy and specific power

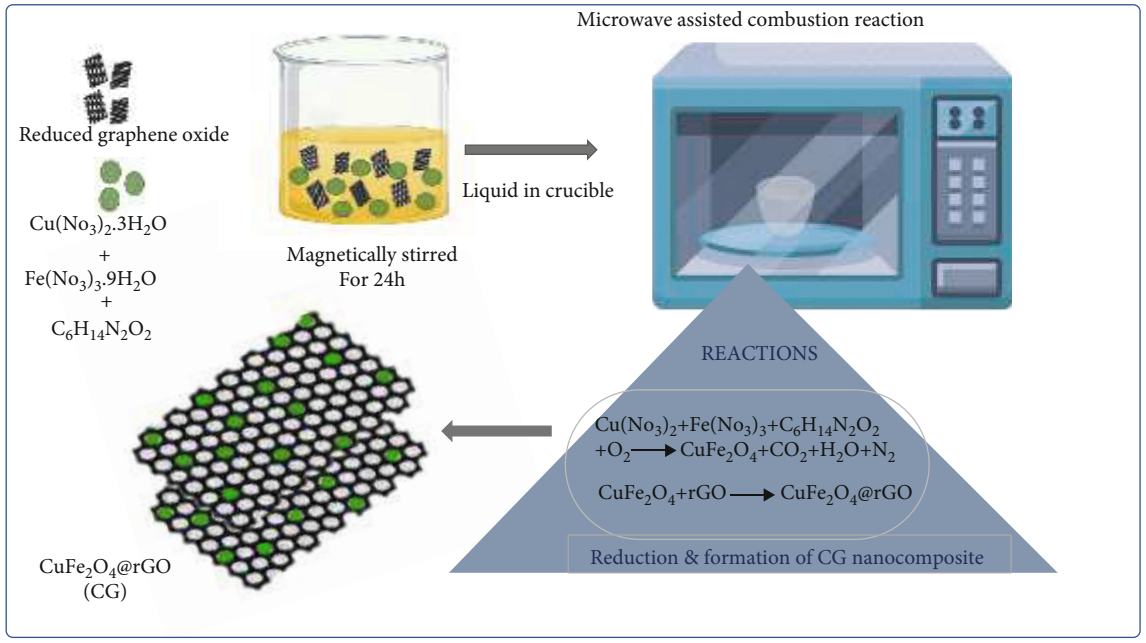

Figure 1: Schematic diagram for the synthesis of $CuFe_2O_4$/rGO (CG) nanocomposite.

of the fabricated electrode are calculated from the equations given below:

$$E = \frac{C \times (\Delta V)^2}{2 \times 3.6} \left(\frac{\text{Wh}}{\text{kg}}\right), \tag{2}$$

$$P = \frac{E \times 3600}{\Delta t} \left(\frac{\text{W}}{\text{kg}}\right), \tag{3}$$

where E is the specific energy (Wh/kg), C is the capacity, ΔV is the applied potential window, P is the specific power (W/kg), and Δt is the discharge time.

3. Results and Discussions

3.1. Structural and Morphological Characterization of CF and CG. The phase purity and crystallographic structure of the prepared sample have been examined by means of X-ray diffraction and Rietveld refinements (see Figure 2). The peaks presented in Figure 2(a) correspond to $CuFe_2O_4$ cubic spinel ferrite with the absence of major impurities. From the literature studies, the GO peaks appear at $2\theta = 10^\circ$ and 43° corresponding to (001) and (002) planes, respectively. Upon reduction of GO, a broad peak at $2\theta = 20^\circ$ corresponding to (002) plane is observed [49]. However, the displayed XRD patterns in Figure 2(b) show the absence of rGO peaks which is because of the exfoliation of GO that occurred in the formation of $CuFe_2O_4$ crystal growth onto the graphene layers. The pattern also matches well with the JCPDS card number 01-072-1174 and 01-077-0010 for the cubic and hexagonal $CuFe_2O_4$ as well as 00-039-1346 and 01-071-0010 for cubic and hexagonal Fe_2O_3, respectively. The phase composition, lattice parameters, crystallite size, and micro-strain along with fitting factors are reported in Table 1. From the results, the lattice parameter of CF is found to be 8.665 Å, whereas that of CG is slightly reduced to 8.393 Å. It is noted that the (311) peak has the highest intensity implying preferential grain growth along the (311) plane.

The crystallite size D (nm) has been estimated by using the Scherrer formula [50]:

$$D = \frac{K\lambda}{\beta \cos \theta}, \tag{4}$$

where λ is the X-ray wavelength (0.1542 nm), K is the Scherrer constant, β is the full width at half maximum (FWHM), and θ is the Bragg angle of the (311) plane. The calculated value of D for $CuFe_2O_4$ phase is found to increase significantly after adding rGO, i.e., 25 nm for CF to 59 nm for CG.

The microstructure of copper ferrite and copper ferrite/rGO composite and their corresponding chemical composition are analyzed by SEM/EDS as illustrated in Figures 3(a)–3(d). The SEM images reveal spherically shaped and monodispersed nanoparticles with relatively uniform size distribution, i.e., 40–70 nm with an average particle size of 62 nm for CF and 50–80 nm with an average particle size of 73 nm for CG (Figure 3(a)). From Figure 3(b), it can be observed that CG NPs are distributed all over rGO sheets; however, some agglomeration is also found, which may be due to the magnetic interaction between the free CF particles and graphene.

The elemental analysis carried out for bare CF and CG nanocomposite confirms the presence of Cu, Fe, and O, as shown in Figures 3(c) and 3(d). The Cu/Fe ratio obtained from EDX is found to be in accordance with the starting stoichiometric elemental ratio for $CuFe_2O_4$ compound. The EDX (Figure 3(d)) spectrum of CG reveals obviously the emergence of C peak, in addition to Fe, Cu, and O elements. The C peak indicates the presence of rGO in the CG

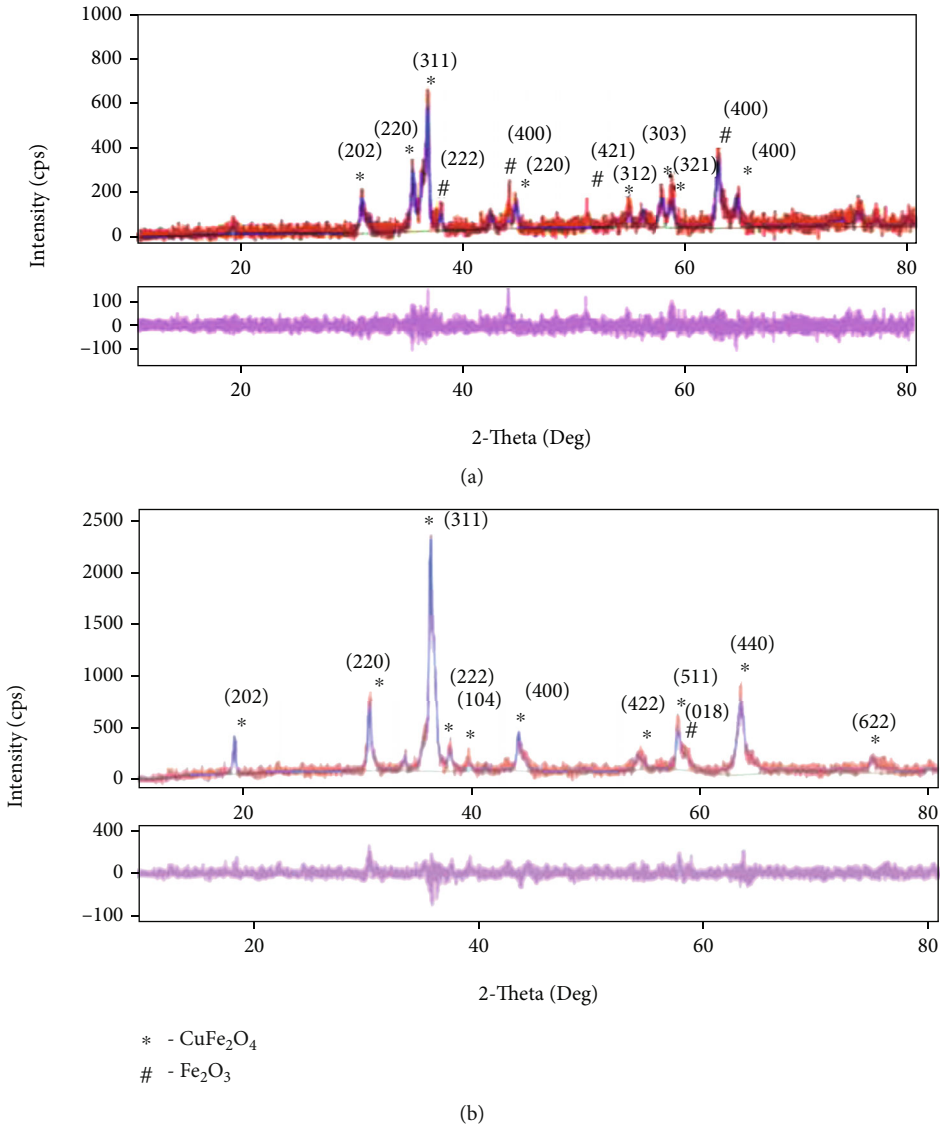

Figure 2: XRD Rietveld refined patterns of (a) CF and (b) CG.

Table 1: Phase composition and structural and microstructural parameters as obtained by the Rietveld refinements of XRD patterns of CF and CG nanocomposite.

Sample	Phase composition (%)	Crystallite size (nm)	Microstrain (%)	Lattice parameters (Å)	Fit parameters
CF	$CuFe_2O_4$ 29 (3)	24.47 (12) 10.25 (18)	0.02 (6) 0.15 (15)	$a = b = 5.829$, $c = 8.665$ (4); $\alpha = \beta = \gamma = 90^\circ$	$R_{wp} = 27.21\%$; $R_e = 10.13$; $R_p = 20.89$
	Fe_2O_3 71 (13)			$a = b = c = 8.377$ (8); $\alpha = \beta = \gamma = 90^\circ$	$S = 2.6826$; $\lambda_2 = 7.1965$
CG	$CuFe_2O_4$ 14 (2)	14.53 (6)	0.15 (5)	$a = b = 2.9795$ (18), $c = 21.10$ (10); $\alpha = \beta = 90$, $\gamma = 120^\circ$	$R_{wp} = 17.64\%$; $R_e = 6.60$; $R_p = 13.69$ $S = 2.6700$; $\lambda_2 = 7.1288$
	Fe_2O_3 4.7 (8)	24.9 (7)	0.14 (2)	$a = b = 5.15$ (3), $c = 13.543$ (12); $\alpha = \beta = 90^\circ$, $\gamma = 120^\circ$	
	$CuFe_2O_4$ 81 (3)	58.8 (12)	0.54 (6)	$a = b = c = 8.393$ (2); $\alpha = \beta = \gamma = 90^\circ$	

R_{wp}: weighted profile R factor; R_e: expected R factor; R_p: profile R factor; S: goodness of fit ($S = R_{wp}/R_e$); $\lambda_2 = S^2$.

nanocomposite. It is important to highlight that there are no additional peaks related to any impurities, thereby confirming the purity of the prepared CF and CG samples [51].

The TEM images displayed in Figures 3(e) and 3(f) reveal the presence of circular platelet nanoparticles for CF and CG with the tendency of agglomeration because rGO

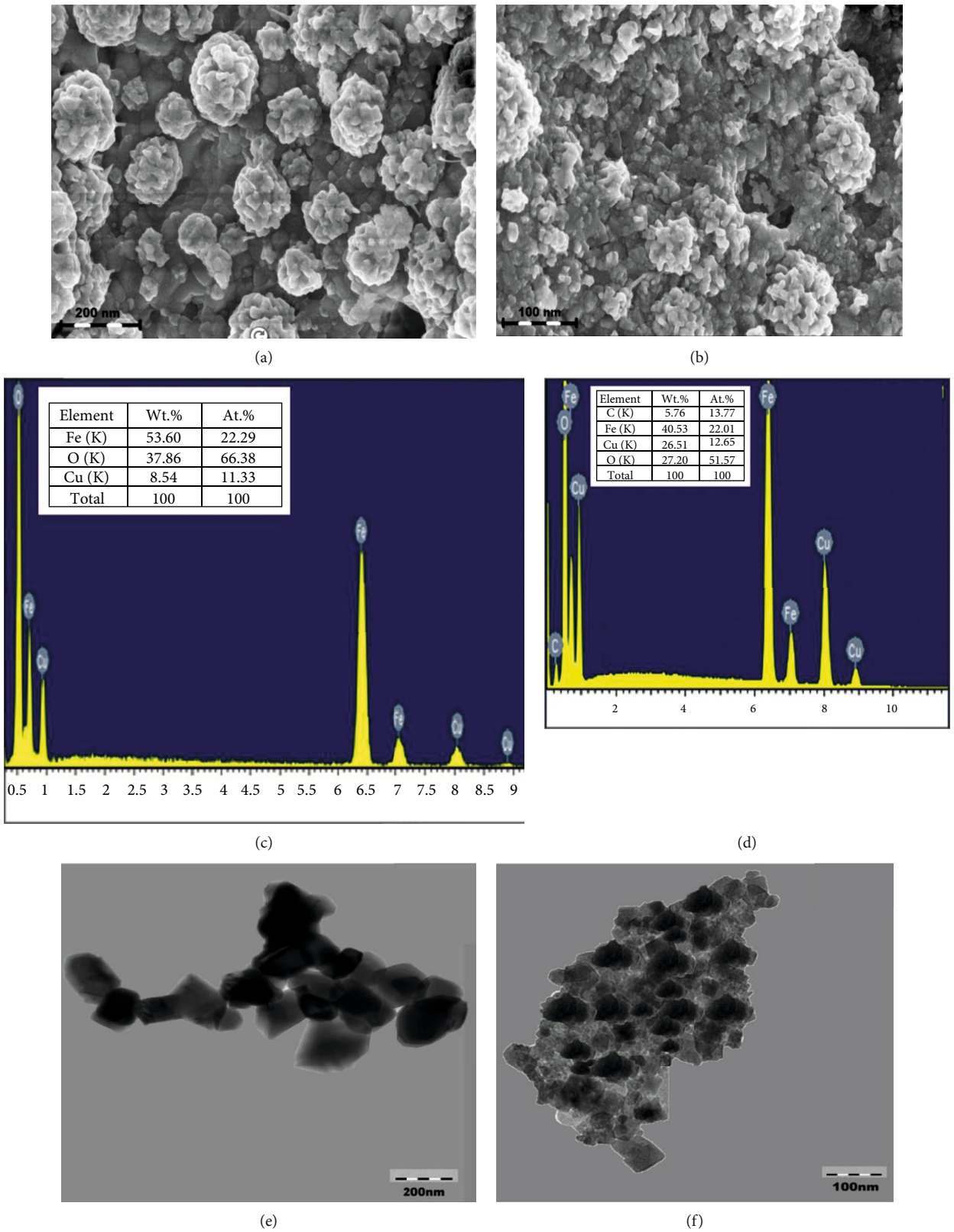

Figure 3: SEM images of (a) CF and (b) CG with the corresponding EDX spectra for (c) CF and (d) CG. TEM images of (e) CF and (f) CG.

forms a graphene-like sheets that are joined together by π-π interaction within the matrix [52]. The particle size distribution estimated from TEM images is in the range 40-60 nm for CF with a mean value of 50 nm, which then increases to 50-90 nm and 74 nm for CG. The smaller particle size of CF when combined with rGO enables enhanced

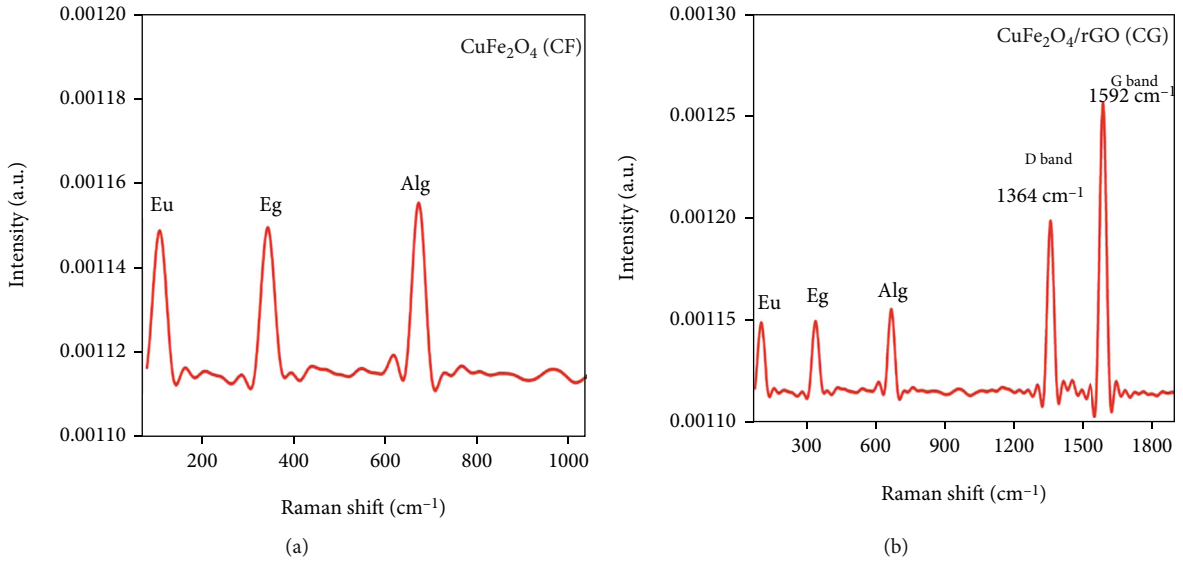

Figure 4: FT-Raman image of (a) CF and (b) CG.

electrochemical performance due to the diffusion of ions and its readiness to undergo cyclic changes.

The estimated particle size from SEM and TEM images matches well, and due to the agglomeration on the surface, the particles appear to be dense. This resulted in the slight variation to that of the calculated crystallite size with the particle size obtained from SEM and TEM images.

Raman analysis has been carried out to measure the chemical structure and to study the phase and molecular interactions of the as-prepared CF and CG samples (see Figure 4). The Raman spectrum of CF shows three vibrational modes around 105, 342, and 670 cm^{-1} corresponding to Eu, Eg, and A1g which is associated with the symmetric stretching caused by the presence of oxygen atoms in the CF. For CG sample, two well-resolved characteristic peaks are presented: a D-band at 1364 cm^{-1} appearing due to the distortion of sp2 carbon atoms by the oxygen groups in the composite and a G-band at 1592 cm^{-1} due to the stretching of C-C bond caused by the graphite in the sample. The I_D/I_G ratio of 0.9 for CG sample manifests the existence of other functional groups, which is favorable for the nanocomposite formation [53, 54].

3.2. Evaluation of the Electrochemical Characteristics of CF and CG Electrodes. The electrochemical behavior and characteristics of pure $CuFe_2O_4$ and $CuFe_2O_4$/rGO nanocomposite samples have been investigated using cyclic voltammetry technique, and the results are presented in Figures 5(a) and 5(b). It is important to notice that the voltametric current increases with the increase in scan rate, indicating the capacitive behavior of both samples. This trend is attributed to the formation of diffusion layer that is hindering the mobility of electrolytic ions to the electrode thereby resulting in lowering the current. Similarly, higher current density is achieved, because of the absence of the formation of diffusion layer near the electrode [55]. The aqueous 6 M KOH electrolyte plays a key role in regulating the charges between the electrodes. The conductivity of aqueous electrolytes is high due to their low viscosity. Hence, the rise in peak intensity is caused by the increased OH^- concentration which shows significant current response of the electrode. This superior capacitive behavior is achieved by the higher conductivity and ionic mobility caused by OH^- ions of the KOH electrolyte. Certainly, the use of aqueous electrolyte possesses small potential window because of the fast water decomposition of the electrolyte [56, 57].

CV curves of both samples show a pair of cathodic and anodic peaks, which manifests the influence of redox reactions due to the OH^- electrolyte ions and an indication of an enhanced pseudocapacitance behavior. Also, it is worth noting the increase in the peak current, which can be associated with the electrochemical kinetic reactions occurring between the electrolyte and the electrode. Figure 5(c) illustrates the comparison of CV curves of the bare nickel foam and the prepared CF and CG electrodes at a scan rate of 5 mV/s in a potential window of 0 to 0.5 V. The bare nickel foam shows no capacitive contribution as it generates negligible amount of current when compared to the prepared CF and CG electrodes. The CV curves of CF and CG show a pair of redox peaks which signify a faradaic capacitive material corresponding to pseudocapacitive behavior. Remarkably, the CG shows high current density and wider area, indicating a significant enhancement in a capacitive behavior than that of CF. This is attributed to the presence of highly conductive GO sheets on the electrode that acts as a backbone to the $CuFe_2O_4$ structure, which provides excellent conductive nature to promote rapid redox reactions. The presence of rGO in the electrode also controls the structural integrity thereby supporting the electrochemical features of the samples [58, 59].

The GCD analysis is considered as the more sensible approach to better understand the supercapacitive features present in a material. The GCD profiles have been recorded in the potential range 0-0.5 V at different current densities

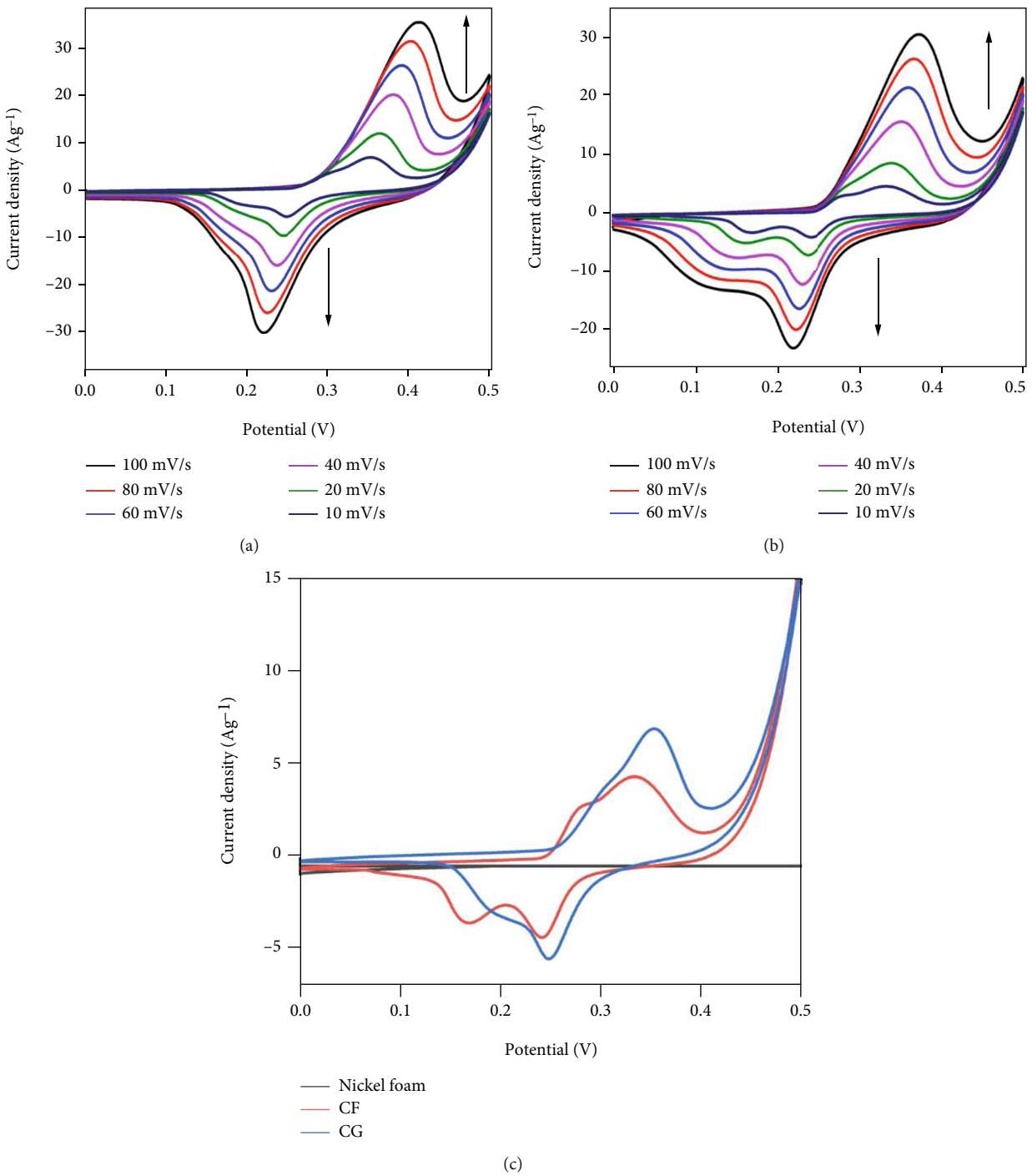

Figure 5: Cyclic voltammograms of (a) (CF) and (b) (CG). (c) Comparison cyclic voltammetry curves of nickel foam, CF, and CG.

from 2 to 10 A/g as presented in Figures 6(a) and 6(b). The specific capacity values are calculated from the GCD profiles for CF and CG electrodes. The CF electrode exhibits 562, 290, 228, 194, and 102 C/g at current density of 2, 4, 6, 8, and 10 A/g, respectively. Significantly, the CG electrode shows higher values, i.e., 800, 600, 431, 350, and 312 C/g at 2, 4, 6, 8, and 10 A/g, respectively. It is interesting to note that the CG electrode displays enhanced specific capacity, which is around 42% increase at a current density of 2 A/g. This enhancement in the capacity associated with the addition of rGO to the $CuFe_2O_4$ matrix considerably intensifies the capacitive nature by interfering with the electrolyte and the prepared electrode [60]. The increase in plateau length of the GCD curve is due to the intensity of redox reaction which is attributed to the KOH electrolyte. From Figure 6(c), it can be seen that the specific capacity obtained from the GCD curves for both CF and CG decreases with the increase in the current density. This is mainly due to the immobile redox reaction kinetics and low perforation of electrolyte ions in and out of the electrode at higher density [26].

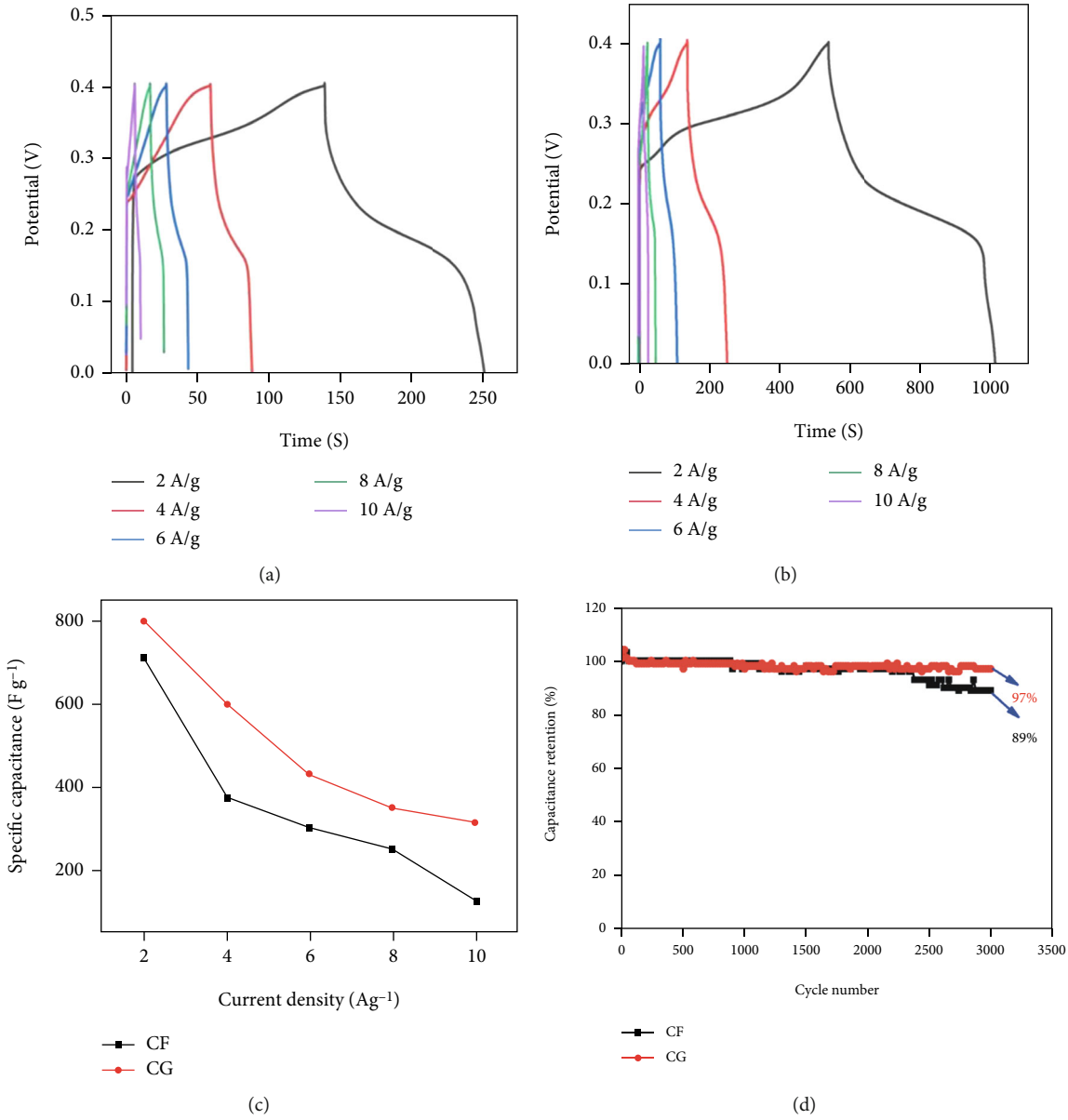

Figure 6: Continued.

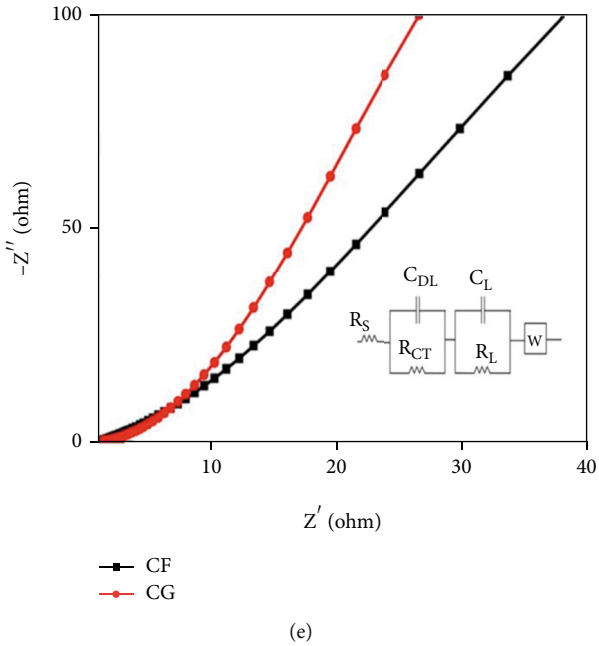

(e)

Figure 6: GCD curves of (a) CF and (b) CG with various applied currents. (c) Variation of the specific capacity of CF and CG electrodes as a function of the current density from 2 to 10 A g^{-1}. (d) Cyclic stability of CF and CG over 3000 cycles in an electrolyte solution of 6 M KOH. (e) Nyquist plot of both CF and CG and the corresponding equivalent circuit as inset.

The cyclic stability is an important factor to inspect the durability of the prepared electrodes. The cyclic stability of CF and CG has been investigated at a constant current density of 10 A/g for 3000 cycles. From Figure 6(d), it is noted that the cyclic stability of CG shows steady capacity while that of CF manifests a slight decrease after the first few cycles. The CG electrode has a capacity fading of ~25% which is much smaller than ~47% for the CF electrode. This enhancement in the cyclic performance of CG electrode is due to the presence of rGO sheets in the composite electrode, since they act as a support against electrolyte ion intercalation/deintercalation while cycling [61].

EIS is an attractive analytical tool to analyze the internal resistive properties of the samples, specifically the solution resistance (R_s) and charge transfer resistance (R_{ct}) arising at the electrode/electrolyte interface. The Nyquist plots of CF and CG electrodes are displayed at the frequency range between 0.01 Hz and 100 kHz, representing the combination of imaginary component (Z'') of the impedance against the real component (Z'). The semicircle in the lower portion of the plot at higher frequency range corresponds to the charge transfer resistance (R_{ct}) of the electrolyte/electrode interface [62]. Hence, the interfacial charge transfer resistance (R_{ct}) can be estimated by measuring the diameter of the semicircle. The internal resistance (R_s) in the plot is obtained from the intercept of semicircle region with the x -axis, which is affected by the combined resistances between the electrode and the electrolyte. The straight line at low-frequency region reveals the diffusion activity known as the Warburg diffusion. From Figure 6(e), CF and CG plots show the absence of semicircle, hence indicating a higher Warburg impedance. This is because of the combined effects associated with higher diffusion of ions and strong resistance towards ions' movement. Similarly, the lower Warburg impedance indicates that the lower-frequency region is more vertical than 45°, which demonstrates a better electrochemical performance of the electrode [24]. The CG composite manifests more vertical trend than CF, which shows that CG has less contact resistance between the copper ferrite and rGO, resulting in a more efficient supercapacitor material. The CG sample shows an R_{ct} value of 1.13 Ω, slightly higher than that for CF which is 1.03 Ω. Further, the lower R_{ct} indicates an enhanced charge transformation of the CG electrode. The equivalent series resistance (ESR) was calculated from first x intercept and slope of Nyquist plot. The figured ESR value for CF is found to be 1.03 Ω and 1.13 Ω for CG. This indicates better conductivity of ions between the electrolyte and the as-prepared electrode materials [63].

3.3. Fabrication of the CG Device. Generally, electrochemical measurements using a two-electrode system are more reliable than a 3-electrode setup. We have fabricated an asymmetric-type capacitor cell using CG and activated carbon as electrodes to test its suitability for SC electrode in device applications. Figure 7(a) illustrates the CV analysis of the fabricated CG device at different scan rates from 10 to 100 mV/s at a potential window of 0 to 1 V in 6 M KOH electrolyte solution. The quasi-rectangular shape of the CV curves manifests a better capacitor behavior of the device. The calculated specific capacity of the device from the GCD measurements is found to decrease gradually with increasing the current density, i.e., 360, 331, 284, 225, 150, and 62 C/g at 1, 2, 4, 6, 8, and 10 A/g, respectively, as shown in Figure 7(b). This is usually attributed to the short

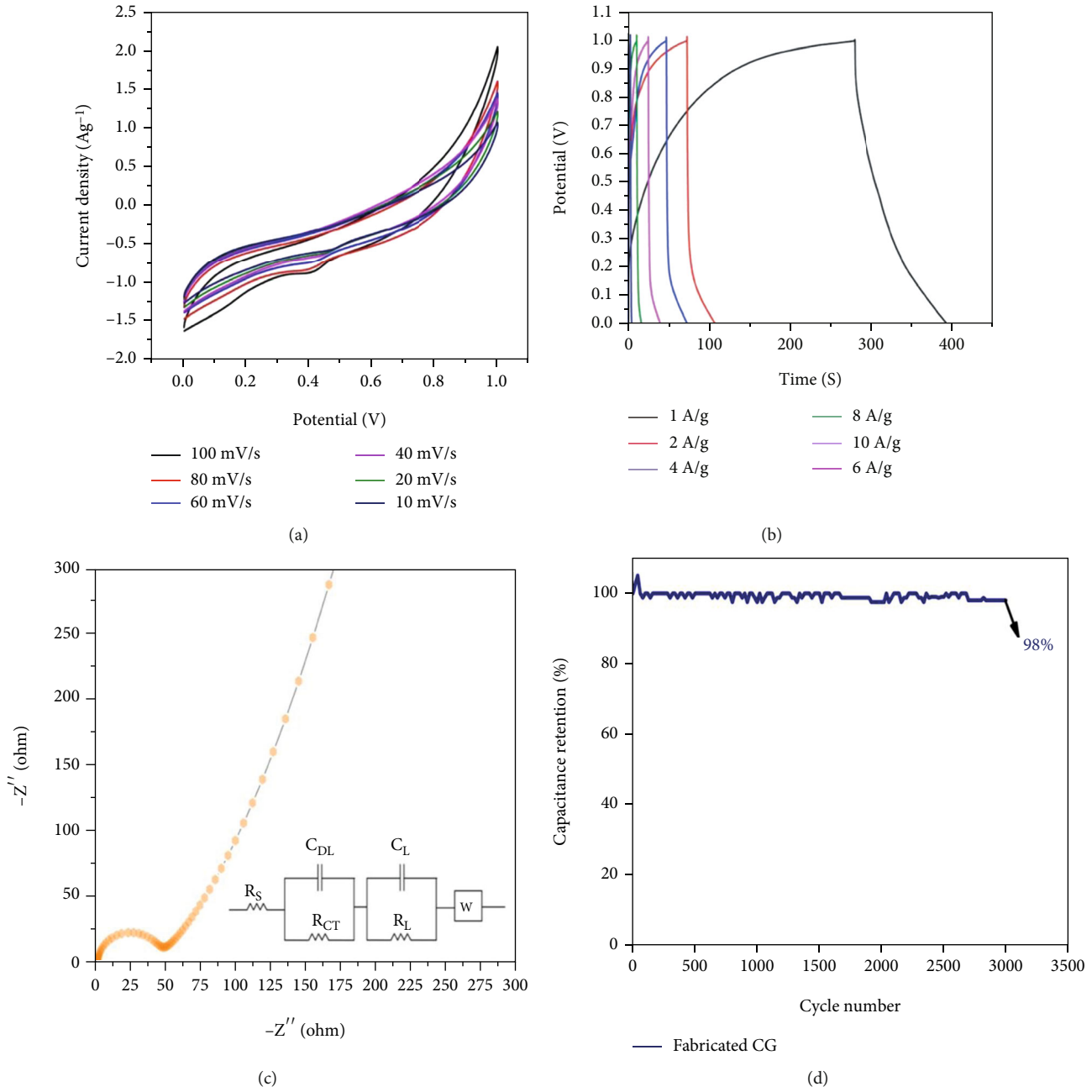

FIGURE 7: (a) CV curves of fabricated CG supercapacitor at different scan rates. (b) GCD curves of fabricated CG supercapacitor at different current densities. (c) Nyquist plot of fabricated CG supercapacitor. (d) Cycling test of fabricated CG supercapacitor at a current density of 1 A g^{-1}.

timeframe of the electrolyte ions which is not enough to enter the innermost part of the electrolyte at higher current density [64]. At the current density of 1 A/g, the as-fabricated device exhibits a specific energy of 18.3 Wh/kg and a specific power of 455 W/kg. The Nyquist plots obtained from EIS measurements of the device are depicted in Figure 7(c), and the R_{ct} value of the CG device is found to be 49 Ω. The cyclic stability of the device is performed at a current density of 10 A g^{-1} for 3000 cycles. Figure 7(d) shows an excellent capacity retention of ~98%. This is due to the presence of high surface area activated carbon as an electrode. The coulombic efficiency of the fabricated CG sample is obtained using the following equation:

$$\eta = \frac{t_D}{t_C} \times 100\%, \tag{5}$$

where t_D is the discharge time and t_C is the charge time in second. The low coulombic efficiency of 78% was recorded for fabricated CG electrode at 1 A/g which is due to the increased rate of side reaction at lower current density [62]. The lower discharge time of the fabricated CG device

Table 2: Comparative study of the present work with literatures.

Material	Synthesis method and precursors	Phase purity	Particle morphology and size (nm)	Capacitance and cyclability	Reference
$CuFe_2O_4$	Microwave method	Pure cubic spinel	Spherical-like morphology (200 nm)	(i) 712 F/g @ 2 A/g (ii) 89% capacitance retention at 10 A/g (iii) 11% loss after 2650 cycles	This work
$CuFe_2O_4$/rGO		Composite		(i) 800 F/g @ 2 A/g (ii) 98% capacitance retention at 10 A/g (iii) 2% loss after 2650 cycles	
$CuFe_2O_4$	Hydrothermal method	Pure cubic spinel	Spherical-like micro-nanostructure morphology (200 nm)	(i) 334 F/g @ 0.6 A/g (ii) 85% capacitance retention at 1 A/g (iii) 12% loss after 600 cycles	[14]
$CuFe_2O_4/Fe_2O_3$	Coprecipitation method	Composite	Spherical-like morphology (100 nm)	(i) 638 F/g @ 0.6 A/g (ii) 66.4% capacitance retention at 1 A/g (287.8 F/g) (iii) For copper ferrite 48.77 F/g @ 0.6 A/g and 21.95 F/g @ 1 A/g (iv) 20% loss after 2000 cycles	[24]
$C/CuFe_2O_4$	Electrospinning method	Composite	Microfiber-like morphology (100 nm)	(i) 191 F/g @ 0.2 A/g (ii) 80% capacitance retention at 1 A/g (iii) 2% loss after 1000 cycles	[61]
$CuFe_2O_4$/GO	Rotational flux chemistry approach	Pure cubic spinel	2D Holey sheet-like morphology (10-20 nm)	(i) 1164 C/g-1940 F/g @ 1 A/g (ii) 98% capacitance retention at 10 A/g (iii) 2% loss after 10000 cycles	[68]
$CuFe_2O_4$/GO	One-pot synthesis method	Composite	Spherical-like morphology	(i) 163 F/g @ 4 A/g (ii) 97% capacitance retention at 2.5 A/g (iii) 3% loss after 10000 cycles	[69]
$CuFe_2O_4$/rGO	Solvothermal method	Composite	Spherical-like morphology (100 nm)	(i) 576.6 F/g @ 1 A/g (ii) 79.1% capacitance retention at 3 A/g (39.4 F/g) (iii) 48.2% loss after 300 cycles	[26]
$CuFe_2O_4$/rGO	Coprecipitation method	Composite	Spherical-like morphology (20 nm)	(i) 797 F/g @ 2 A/g (ii) 92% capacitance retention at 6 A/g (83.9 F/g) (iii) 8.2% loss after 2000 cycles	[48]
$CuFe_2O_4$/rGO	One-step thermochemical method	Composite	Spherical-like morphology	(i) 1190 mAh/g @ 100 mA/g (ii) 58.6% capacitance retention at 100 mA/g (iii) 41.4% loss after 2000 cycles	[29]

than the charge time is because of the lower coulombic efficiency.

3.4. Comparison with Literature. The electrochemical performances of both CF and CG composites of the present work are compared with previous studies in the literature. Zhu et al. [14] reported the solvothermal synthesis of $CuFe_2O_4$ with a specific capacitance of 334 F/g in 1 M KOH at 6 A/g, which is attributed to the increase in the rate of OH^- ions diffusing into $CuFe_2O_4$ electrode with the current density. Zhang et al. [25] demonstrated the solvothermal synthesis of copper ferrite-attached graphene nanosheet ($CuFe_2O_4$-GN) with a marked specific capacitance of 576.6 F/g at 1 A/g in 3 M KOH solution, due to the π-π interaction between GN and $CuFe_2O_4$ as well as the higher diffusing rate of electrolyte ions with decreasing current density. Similarly, Khan et al. [24] suggested the use of $CuFe_2O_4$-Fe_2O_3 nanocomposite prepared by coprecipitation with a much higher capacitance of 638.24 F/g at 1 A/g in 1 M H_2SO_4 electrolyte which is associated with the short diffusion of pathway of ions, higher surface area, and increased electrical conductivity of the composite. Nilmoug et al. [64] reported on $C/CuFe_2O_4$ composite prepared via electrospinning and carbonization with a low capacitance of 191 F/g at 10 mV/s in 1 M KOH electrolyte solution which is due to the high-rate capability and capacity due to the fast movement of charge carriers on the electrode surface. Chandel et al. [26] proposed $CuFe_2O_4$/rGO preparation by coprecipitation with the highest specific capacitance of 792 F/g at 2 A/g in 3 M KOH; i.e., the decrease of the ionic diffusion resistance of the electrolyte ions enhances the redox kinetic, and thereby, the capacitance increases. Moreover, asymmetric supercapacitors have attracted significant attention with the use of carbon-based electrode materials due to improved cycle lifetime and good power output. Chen et al. fabricated porous carbon derived from bamboo, with boron and nitrogen codoped

materials as electrode materials. The resulting asymmetric supercapacitor exhibited specific capacitance of 318 F/g at 0.2 A/g with energy density of 37.8 Wh kg^{-1} in 1 M KOH electrolyte [35]. Yu et al. prepared carbon-based asymmetric supercapacitor electrode materials with nitrogen-doped carbon materials derived from ginkgo leaf. In this study, the obtained specific capacitance is 345 F/g at 0.2 A/g [65]. In a similar study, Zhu et al. prepared a KOH-activated carbon electrode material obtained from ginkgo leaf for asymmetric supercapacitor and reported improved specific capacitance of 374 F/g at 0.5 A/g [66]. Another high-performance flexible carbon-based electrode material was fabricated from carbon felt with KOH and potassium argininate (AKCF) as activators which were reported by Tao et al. [67]. The study reported a specific capacity of 403 C/g with high energy density of 68.4 Wh/kg. A comparative study of the present work with literatures is represented in Table 2. It can be highlighted that the newly proposed facile method for the preparation of $CuFe_2O_4$ and $CuFe_2O_4$/rGO from a commercially available microwave is cost-effective, facile, and fast. The as-synthesized $CuFe_2O_4$ and $CuFe_2O_4$/rGO deliver an excellent specific capacity of 712 and 800 C/g, respectively, at 2 A/g in 6 M KOH solution. The fabricated CG device demonstrates promising features, specific energy of 18.3 Wh/kg, with a specific power of 455 W/kg and with 98% of capacity retention. The achieved maximum specific capacity of 800 C/g of CG electrode is greater than the reported results of carbon-based asymmetric electrode materials and moreover is comparable in terms of simple and cost-effective preparation of graphene-based electrodes.

4. Conclusion

In this study, copper ferrite and copper ferrite/rGO nanocomposite as an active material were synthesized via the microwave combustion method for supercapacitor applications. The copper ferrite is evenly scattered onto rGO sheets and subsequently increases the electrical conductivity performance the composite $CuFe_2O_4$/rGO. In 6 M KOH electrolyte, the CG exhibited a high capacity of 800 C/g at 2 A/g compared to 712 C/g for CF. The enhancement in the specific capacity resulted from the low interfacial charge transfer resistance. To the best of authors' knowledge, this is the first microwave synthesis route of $CuFe_2O_4$ and $CuFe_2O_4$/rGO with high specific capacity at lower current density. The fabricated CG device demonstrates a specific capacity of 360 C/g at 1 A/g current density with a resistance of 50 Ω, with a specific energy of 18.3 Wh/kg, and with a specific power of 455 W/kg while maintaining an excellent cyclic stability, i.e., 98% capacity retention at current density of 1 A/g after 3000 cycles. The results suggest that the prepared nanocomposite is an effective and a promising high-performance supercapacitor for energy storage device owing to its low-cost and environmentally friendly source materials.

Data Availability

No data were used to support this study.

Conflicts of Interest

The authors have no conflict of interest to declare that is relevant to the content of the article.

Acknowledgments

The authors would like to acknowledge Loyola College Management, affiliated to University of Madras, for presuming the necessary organizational facilities to carry out the research work.

References

[1] M. B. Askari and P. Salarizadeh, "Binary nickel ferrite oxide ($NiFe_2O_4$) nanoparticles coated on reduced graphene oxide as stable and high-performance asymmetric supercapacitor electrode material," *International Journal of Hydrogen Energy*, vol. 45, no. 51, pp. 27482–27491, 2020.

[2] Y. Shao, M. F. El-Kady, J. Sun et al., "Design and mechanisms of asymmetric supercapacitors," *Chemical Reviews*, vol. 118, no. 18, pp. 9233–9280, 2018.

[3] P. Lamba, P. Singh, P. Singh et al., "Recent advancements in supercapacitors based on different electrode materials: classifications, synthesis methods and comparative performance," *Journal of Energy Storage*, vol. 48, article 103871, 2022.

[4] M. Gidwani, A. Bhagwani, and N. Rohra, "Supercapacitors: the near future of batteries," *International Journal of Engineering Inventions*, vol. 4, pp. 22–27, 2014.

[5] Q. Li, S. Zheng, Y. Xu, H. Xue, and H. Pang, "Ruthenium based materials as electrode materials for supercapacitors," *Chemical Engineering Journal*, vol. 333, pp. 505–518, 2018.

[6] Y. Wu, H. Chen, Y. Lu et al., "Rational design of cobalt-nickel double hydroxides for flexible asymmetric supercapacitor with improved electrochemical performance," *Journal of Colloid and Interface Science*, vol. 581, no. Part B, pp. 455–464, 2021.

[7] Y. Tao, Y. Wu, H. Chen et al., "Synthesis of amorphous hydroxyl-rich Co_3O_4 for flexible high-rate supercapacitor," *Chemical Engineering Journal*, vol. 396, article 125364, 2020.

[8] Y. Ma, X. Zhu, B. Wang et al., "Sacrificial template synthesis of hierarchical nickel hydroxidenitrate hollow colloidal particles for electrochemical energy storage," *Chemical Engineering Science*, vol. 217, 2020.

[9] X. Zhu, Y. Wu, Y. Lu et al., "Aluminum-doping-based method for the improvement of the cycle life of cobalt-nickel hydroxides for nickel-zinc batteries," *Journal of Colloid and Interface Science*, vol. 587, pp. 693–702, 2021.

[10] B. Bhujun, M. T. T. Tan, and A. S. Shanmugam, "Study of mixed ternary transition metal ferrites as potential electrodes for supercapacitor applications," *Results in Physics*, vol. 7, pp. 345–353, 2017.

[11] K. Malaie and M. R. Ganjali, "Spinel nano-ferrites for aqueous supercapacitors; linking abundant resources and low-cost processes for sustainable energy storage," *Journal of Energy Storage*, vol. 33, article 102097, 2021.

[12] N. Kumar, A. Kumar, G. M. Huang, W. W. Wu, and T. Y. Tseng, "Facile synthesis of mesoporous $NiFe_2O_4$/CNTs nanocomposite cathode material for high performance asymmetric pseudocapacitors," *Applied Surface Science*, vol. 433, pp. 1100–1112, 2018.

[13] R. Lakra, R. Kumar, P. K. Sahoo, D. Thatoi, and A. Soam, "A mini-review: graphene based composites for supercapacitor application," *Inorganic Chemistry Communications*, vol. 133, article 108929, 2021.

[14] M. Zhu, D. Meng, C. Wang, and G. Diao, "Facile fabrication of hierarchically porous $CuFe_2O_4$ nanospheres with enhanced capacitance property," *ACS Applied Materials & Interfaces*, vol. 5, no. 13, pp. 6030–6037, 2013.

[15] J. Wang, Q. Deng, M. Li et al., "Copper ferrites@reduced graphene oxide anode materials for advanced lithium storage applications," *Scientific Reports*, vol. 7, no. 1, pp. 1–12, 2017.

[16] Y. Fu, Q. Chen, M. He et al., "Copper ferrite-graphene hybrid: A multifunctional heteroarchitecture for photocatalysis and energy storage," *Industrial & Engineering Chemistry Research*, vol. 51, no. 36, pp. 11700–11709, 2016.

[17] L. Luo, R. Cui, H. Qiao et al., "High lithium electroactivity of electrospun $CuFe_2O_4$ nanofibers as anode material for lithium-ion batteries," *Electrochimica Acta*, vol. 144, pp. 85–91, 2014.

[18] M. L. Aparna, A. N. Grace, P. Sathyanarayanan, and N. K. Sahu, "A comparative study on the supercapacitive behaviour of solvothermally prepared metal ferrite (MFe_2O_4, M = Fe, Co, Ni, Mn, Cu, Zn) nanoassemblies," *Journal of Alloys and Compounds*, vol. 745, pp. 385–395, 2018.

[19] K. Muthukumar, D. S. Lakshmi, S. D. Acharya, S. Natarajan, A. Mukherjee, and H. C. Bajaj, "Solvothermal synthesis of magnetic copper ferrite nano sheet and its antimicrobial studies," *Materials Chemistry and Physics*, vol. 209, pp. 172–179, 2018.

[20] N. Masunga, B. B. Mamba, Y. W. Getahun et al., "Synthesis of single-phase superparamagnetic copper ferrite nanoparticles using an optimized coprecipitation method," *Materials Science and Engineering B*, vol. 272, article 115368, 2021.

[21] V. Kotsyubynsky, R. Zapukhlyak, V. Boychuk et al., "Hydrothermally synthesized $CuFe_2O_4$/rGO and $CuFe_2O_4$/porous carbon nanocomposites," *Applied Nanoscience*, pp. 1–8, 2021.

[22] V. A. Zhuravlev, R. V. Minin, V. I. Itin, and I. Y. Lilenko, "Structural parameters and magnetic properties of copper ferrite nanopowders obtained by the sol-gel combustion," *Journal of Alloys and Compounds*, vol. 692, pp. 705–712, 2017.

[23] L. Jin, Y. Qiu, H. Deng, W. Li, H. Li, and S. Yang, "Hollow $CuFe_2O_4$ spheres encapsulated in carbon shells as an anode material for rechargeable lithium-ion batteries," *Electrochimica Acta*, vol. 56, no. 25, pp. 9127–9132, 2011.

[24] R. Khan, M. Habib, M. A. Gondal et al., "Facile synthesis of $CuFe_2O_4$–Fe_2O_3 composite for high-performance supercapacitor electrode applications," *Materials Research Express*, vol. 4, no. 10, pp. 2088–2098, 2017.

[25] W. Zhang, B. Quan, C. Lee et al., "One-step facile solvothermal synthesis of copper ferrite-graphene composite as a high-performance supercapacitor material," *ACS Applied Materials & Interfaces*, vol. 7, no. 4, pp. 2404–2414, 2015.

[26] M. Chandel, D. Moitra, P. Makkar, H. Sinha, H. S. Hora, and N. N. Ghosh, "Synthesis of multifunctional $CuFe_2O_4$–reduced graphene oxide nanocomposite: an efficient magnetically separable catalyst as well as high performance supercapacitor and first-principles calculations of its electronic structures," *RSC Advances*, vol. 8, no. 49, pp. 27725–27739, 2018.

[27] Z. Xing, Z. Jun, J. Yang, H. Xu, and Y. Qian, "One-step solid state reaction to selectively fabricate cubic and tetragonal $CuFe_2O_4$ anode material for high power lithium ion batteries," *Electrochimica Acta*, vol. 102, pp. 51–57, 2013.

[28] V. Elayappan, S. Muthusamy, G. Mayakrishnan et al., "Ultrasonication-dry-based synthesis of gold nanoparticle-supported CuFe on rGO nanosheets for competent detection of biological molecules," *Applied Surface Science*, vol. 531, article 147415, 2020.

[29] S. A. Soomro, I. H. Gul, H. Naseer, S. Marwat, and M. Mujahid, "Improved performance of $CuFe_2O_4$/rGO nanohybrid as an anode material for lithium-ion batteries prepared via facile one-step method," *Current Nanoscience*, vol. 15, no. 4, pp. 420–429, 2019.

[30] C. An, Y. Zhang, H. Guo, and Y. Wang, "Metal oxide-based supercapacitors: progress and prospectives," *Nanoscale Adv*, vol. 1, no. 12, pp. 4644–4658, 2019.

[31] S. Ambika, S. Gopinath, K. Saravanan, K. Sivakumar, C. Ragupathi, and T. A. Sukantha, "Structural, morphological and optical properties and solar cell applications of thioglycolic routed nano cobalt oxide material," *Energy Reports*, vol. 5, pp. 305–309, 2019.

[32] B. Bashir, A. Rahman, H. Sabeeh et al., "Copper substituted nickel ferrite nanoparticles anchored onto the graphene sheets as electrode materials for supercapacitors fabrication," *Ceramics International*, vol. 45, no. 6, pp. 6759–6766, 2019.

[33] O. Akhavan, "The effect of heat treatment on formation of graphene thin films from graphene oxide nanosheets," *Carbon*, vol. 48, no. 2, pp. 509–519, 2010.

[34] G. Lou, G. Pei, Y. Wu et al., "Combustion conversion of wood to N, O co-doped 2D carbon nanosheets for zinc-ion hybrid supercapacitors," *Chemical Engineering Journal*, vol. 413, article 127502, 2021.

[35] H. Chen, Y. Zheng, X. Zhu et al., "Bamboo-derived porous carbons for Zn-ion hybrid supercapacitors," *Materials Research Bulletin*, vol. 139, article 111281, 2021.

[36] D. Thatikayala and B. Min, "Copper ferrite supported reduced graphene oxide as cathode materials to enhance microbial electrosynthesis of volatile fatty acids from CO_2," *Science of The Total Environment*, vol. 768, article 144477, 2021.

[37] C. R. Patra, G. Alexandra, S. Patra et al., "Microwave approach for the synthesis of rhabdophane-type lanthanide orthophosphate (Ln = La, Ce, Nd, Sm, Eu, Gd and Tb) nanorods under solvothermal conditions," *New Journal of Chemistry*, vol. 29, no. 5, pp. 733–739, 2005.

[38] O. Palchik, I. Felner, G. Kataby, and A. Gedanken, "Amorphous iron oxide prepared by microwave heating," *Journal of Materials Research*, vol. 15, no. 10, pp. 2176–2181, 2000.

[39] I. N. Pulidindi, B. B. Kimchi, and A. Gedanken, "Can cellulose be a sustainable feedstock for bioethanol production?," *Renewable Energy*, vol. 71, pp. 77–80, 2014.

[40] V. Vasanthi, A. Shanmugavani, C. Sanjeeviraja, and R. Kalai Selvan, "Microwave assisted combustion synthesis of $CdFe_2O_4$: magnetic and electrical properties," *Journal of Magnetism and Magnetic Materials*, vol. 324, no. 13, pp. 2100–2107, 2012.

[41] S. Nain, R. Singh, and S. Ravichandran, "Importance of microwave heating in organic synthesis," *Advanced Journal of Chemistry-Section A*, vol. 2, pp. 94–104, 2019.

[42] M. Sundararajan, L. J. Kennedy, U. Aruldoss, S. K. Pasha, J. J. Vijaya, and S. Dunn, "Microwave combustion synthesis of zinc substituted nanocrystalline spinel cobalt ferrite: structural and magnetic studies," *Materials Science in Semiconductor Processing*, vol. 40, pp. 1–10, 2015.

[43] H. Astaraki, S. M. Masoudpanah, and S. Alamolhoda, "Effects of fuel contents on physicochemical properties and

photocatalytic activity of $CuFe_2O_4$/reduced graphene oxide (RGO) nanocomposites synthesized by solution combustion method," *Journal of Materials Research and Technology*, vol. 9, no. 6, pp. 13402–13410, 2020.

[44] A. Nasiri, M. Nasiri, S. Nouhi, and S. Khodadadian, "Nanocrystalline copper ferrite: synthesis of different shapes through a new method and its photocatalyst application," *Journal of Materials Science: Materials in Electronics*, vol. 28, no. 3, pp. 2401–2406, 2017.

[45] S. P. Schwaminger, P. F. García, G. K. Merck et al., "Nature of interactions of amino acids with bare magnetite nanoparticles," *Journal of Physical Chemistry C*, vol. 119, no. 40, pp. 23032–23041, 2015.

[46] K. Pušnik, T. Goršak, M. Drofenik, and D. Makovec, "Synthesis of aqueous suspensions of magnetic nanoparticles with the co-precipitation of iron ions in the presence of aspartic acid," *Journal of Magnetism and Magnetic Materials*, vol. 413, pp. 65–75, 2016.

[47] A. Shanmugavani, R. Kalai Selvan, S. Layek, and C. Sanjeeviraja, "Size dependent electrical and magnetic properties of $ZnFe_2O_4$ nanoparticles synthesized by the combustion method: comparison between aspartic acid and glycine as fuels," *Journal of Magnetism and Magnetic Materials*, vol. 354, pp. 363–371, 2014.

[48] N. Cao and Y. Zhang, "Study of reduced graphene oxide preparation by Hummer's method and related characterization," *Journal of Nanomaterials*, vol. 2015, Article ID 168125, 2015.

[49] R. Dhanda and M. Kidwai, "Magnetically separable $CuFe_2O_4$/reduced graphene oxide nanocomposites: as a highly active catalyst for solvent free oxidative coupling of amines to imines," *RSC Advances*, vol. 6, no. 58, pp. 53430–53437, 2016.

[50] B. N. Sapna, V. Kumar, and S. K. Singh, "X-ray analysis of $NiFe_2O_4$ nanoparticles by Williamson-Hall and size-strain plot method," *Journal of Advanced Physics*, vol. 6, no. 4, pp. 492–495, 2017.

[51] A. V. Nakhate and G. D. Yadav, "Solvothermal synthesis of $CuFe_2O_4$@rGO: efficient catalyst for C-O cross coupling and N-arylation reaction under ligand free condition," *Chemistry Select*, vol. 2, pp. 7150–7159, 2017.

[52] A. T. Smith, A. M. Lachnce, S. Zeng, B. Liu, and L. Sun, "Synthesis, properties, and applications of graphene oxide/reduced graphene oxide and their nanocomposites," *Nano Materials Science*, vol. 1, no. 1, pp. 31–47, 2019.

[53] L. Zheng, L. Guan, G. Yang, S. Chen, and H. Zheng, "One-pot synthesis of $CoFe_2O_4$/rGO hybrid hydrogels with 3D networks for high capacity electrochemical energy storage devices," *RSC Advances*, vol. 8, no. 16, pp. 8607–8614, 2018.

[54] S. Petnikota, V. V. S. S. Srikanth, P. Nithyadharseni, M. V. Reddy, S. Adams, and B. V. R. Chowdari, "Exfoliated graphene oxide/MoO_2 composites as anode materials in lithium-ion batteries: an insight into intercalation of Li and conversion mechanism of MoO_2," *ACS Applied Materials & Interfaces*, vol. 8, no. 17, pp. 10884–10896, 2016.

[55] P. Makkar and N. N. Ghosh, "Facile synthesis of $MnFe_2O_4$ hollow sphere-reduced graphene oxide nanocomposites as electrode materials for all-solid-state flexible high-performance asymmetric supercapacitors," *ACS Appl Energy Mater*, vol. 3, no. 3, pp. 2653–2664, 2020.

[56] D. Gao, Z. Luo, C. Liu, and S. Fan, "A survey of hybrid energy devices based on supercapacitors," *Green Energy Environment*, 2022.

[57] B. Pal, S. Yang, S. Ramesh, V. Thangadurai, and R. Jose, "Electrolyte selection for supercapacitive devices: a critical review," *Nanoscale Adv*, vol. 1, no. 10, pp. 3807–3835, 2019.

[58] L. Q. Mai, F. Yang, Y. L. Zhao, X. Xu, L. Xu, and Y. Z. Luo, "Hierarchical $MnMoO_4$/$CoMoO_4$ heterostructured nanowires with enhanced supercapacitor performance," *Nature Communications*, vol. 2, no. 1, p. 381, 2011.

[59] L. Xia, S. Wang, G. Liu et al., "Flexible SnO_2/N-doped carbon nanofiber films as integrated electrodes for lithium-ion batteries with superior rate capacity and long cycle life," *Small*, vol. 12, no. 7, pp. 853–859, 2016.

[60] V. T. Le, H. Kim, A. Ghosh et al., "Coaxial fiber supercapacitor using all-carbon material electrodes," *ACS Nano*, vol. 7, no. 7, pp. 5940–5947, 2013.

[61] A. Di Fabio, A. Giorgi, M. Mastragostino, and F. Soavi, "Carbon-poly (3-methylthiophene) hybrid supercapacitors," *Journal of the Electrochemical Society*, vol. 148, no. 8, pp. A845–A850, 2001.

[62] H. Zhang, A. Xie, C. Wang, H. Wang, Y. Shen, and X. Tian, "Bifunctional reduced graphene oxide/V_2O_5 composite hydrogel: fabrication, high performance as electromagnetic wave absorbent and supercapacitor," *Chem Phys Chem*, vol. 15, no. 2, pp. 366–373, 2014.

[63] M. Z. Ansari, N. Parveen, D. K. Nandi et al., "Enhanced activity of highly conformal and layered tin sulfide (SnS_x) prepared by atomic layer deposition (ALD) on 3D metal scaffold towards high performance supercapacitor electrode," *Scientific Reports*, vol. 9, no. 1, p. 10225, 2019.

[64] S. Nilmoug, T. Sinprachim, I. Kotutha et al., "Electrochemical energy storage performance of electrospun $CoMn_2O_4$ nanofibers," *Journal of Alloys and Compounds*, vol. 692, pp. 59–66, 2017.

[65] S. Yu, X. Zhu, G. Lou et al., "Sustainable hierarchical porous biomass carbons enriched with pyridinic and pyrrolic nitrogen for asymmetric supercapacitor," *Materials and Design*, vol. 149, pp. 184–193, 2018.

[66] X. Zhu, S. Yu, K. Xu et al., "Sustainable activated carbons from dead ginkgo leaves for supercapacitor electrode active materials," *Chemical Engineering Science*, vol. 181, pp. 36–45, 2018.

[67] Y. Tao, W. Liu, Z. Li et al., "Boosting supercapacitive performance of flexible carbon via surface engineering," *Journal of Colloid and Interface Science*, vol. 602, pp. 636–645, 2021.

[68] S. B. Bandgar, M. M. Vadiyar, U. P. Suryawanshi, C. L. Jambhale, J. Kim, and S. S. Kolekar, "Rotational reflux chemistry approach derived flat holey $CuFe_2O_4$ nanosheets for supercapacitors application," *Materials Letters*, vol. 279, article 128514, 2020.

[69] P. Makkar, D. Gogoi, D. Roy, and N. N. Ghosh, "Dual-purpose $CuFe_2O_4$-rGO-based nanocomposite for asymmetric flexible supercapacitors and catalytic reduction of nitroaromatic derivatives," *ACS Omega*, vol. 6, no. 43, pp. 28718–28728, 2021.